Prediction of wave ripple characteristics using genetic programming

Evan B. Goldstein*[1], Giovanni Coco[2], A. Brad Murray[1]

[1]Division of Earth and Ocean Sciences, Nicholas School of the Environment; Center for Nonlinear and Complex Systems, Duke University, Box 90227, Durham, NC 27708

[2]Environmental Hydraulics Institute, "IH Cantabria", c /Isabel Torres nº 15., Universidad de Cantabria, Santander, Spain 39011.

*corresponding author: evan.goldstein@unc.edu

Keywords: Ripples; Bedforms; Genetic programming; Machine learning; Data driven Prediction; Symbolic regression

Cite as: E. B. Goldstein, G. Coco, A. B. Murray, 2013. Prediction of wave ripple characteristics using genetic programming, Continental Shelf Research, V. 71, p.1-15, https://doi.org/10.1016/j.csr.2013.09.020.

Abstract

We integrate published data sets of field and laboratory experiments of wave ripples and use genetic programming, a machine learning paradigm, in an attempt to develop a universal equilibrium predictor for ripple wavelength, height, and steepness. We train our genetic programming algorithm with data selected using a maximum dissimilarity selection routine. Thanks to this selection algorithm we use less data to train the genetic programming software, allowing more data to be used as testing (i.e. to compare our predictor vs. common prediction schemes). Our resulting predictor is smooth and physically meaningful, different from other machine learning derived results. Furthermore our predictor incorporates wave orbital ripples that were previously excluded from empirical prediction schemes, notably ripples in coarse sediment and long wavelength, low height ripples ('hummocks'). This new predictor shows ripple length to be a weakly nonlinear function of both bottom orbital excursion and grain size. Ripple height and steepness are both nonlinear functions of grain size and predicted ripple length (i.e. bottom orbital excursion and grain size). We test this new prediction scheme against common (and recent) predictors and the new predictors yield a lower normalized root mean squared error using the testing data. This study further demonstrates the applicability of machine learning techniques to successfully develop well performing predictors if data sets are large in size, extensive in scope, multidimensional, and nonlinear.

1. Introduction

Sufficiently strong water wave propagation over a moveable bed composed of sand grains results in the development rhythmic bedforms whose crest spacing is of the order of centimeters to meters while heights are of the order of centimeters. These features are often termed vortex ripples because of a recirculation cell that develops on the lee side of the bedform that is subsequently ejected upward during reversals in flow direction. Accurate prediction of vortex ripple size and shape is crucial for successful determination of seabed bottom roughness, a first order control on wave attenuation (e.g., Ardhuin et al., 2002), as well as sediment transport as suspended load (e.g., Green and Black, 1999; Bolaños et al., 2012). Furthermore ripple migration is a fundamental mechanism of bedload transport (e.g., Traykovski et al 1999; Becker et al., 2007), and parameterizations of bedload flux necessitate an accurate depiction of ripple size and shape.

Many predictors of equilibrium ripple geometry have been developed from field and laboratory datasets (e.g. Clifton, 1976; Nielsen, 1981; Grant and Madsen, 1982; Wiberg and Harris, 1994; Faraci and Foti, 2002; Styles and Glenn, 2002; Grasmeijer and Kleinhans, 2004; Soulsby and Whitehouse, 2005; Soulsby et al., 2012; Pedocchi and García, 2009a; Camenen, 2009). Equilibrium ripple size and shape is frequently broken down to include 3 subpopulations, a convention developed by Clifton (1976), and reviewed here in order of increasing hydrodynamic forcing. Orbital ripples are believed to scale linearly with wave orbital diameter at the seabed and display the largest steepness (ripple height/wavelength ~ 0.15). Suborbital ripples show spacing that depends on wave orbital diameter and grain size. In even stronger hydrodynamic conditions anorbital ripples form, whose size is related to grain size alone and whose scaling is irrespective of wave orbital diameter. Suborbital ripples link the population of anorbital ripples with those of orbital ripples.

As noted by Smith and Wiberg (2006), recent field and laboratory work has challenged the existing typology for wave-generated ripples as a result of the addition of two new populations (Figure 1). The first are ripples measured in fine sand under strong hydrodynamic conditions. Field and laboratory campaigns in more energetic conditions have discovered the presence of long wavelength, low amplitude ripples ('hummocks') in fine sands that scale with orbital diameter (e.g. Hanes et al., 2001, O'Donoghue et al., 2006). Predictors are unable to accurately capture this ripple size and shape (e.g. Bolaños et al., 2012), yet modeling (Chang and Hanes, 2004) and observation (Green and Black, 1999; Cummings et al., 2009) of these bedforms show they eject vortices and are therefore important for their influence on seabed roughness and sediment transport. Furthermore at times these long wavelength ripples have superimposed anorbital ripples (e.g. Southard et al., 1990; Hanes et al., 2001; Williams et al., 2004), another unsolved problem in wave ripple prediction. Because of these complications, Pedocchi and García (2009a), who developed a recent well performing predictor, omit long wavelength ripples from their analysis, but note that these long wavelength 'round crested' ripples are observed above a critical threshold in U/w_s (where U is the maximum orbital velocity at the bed and w_s is the sediment fall velocity). Dumas et al. (2005) and Cummings et al. (2009) also show that the transition from anorbital scale ripples to round crested long wave orbital scale ripples is a function of orbital velocity (a set value for their given sediment mixtures).

The second new population of ripples are those found in medium to coarse sand (Traykovski et al., 1999; Ardhuin et al., 2002; Becker et al., 2007; Masselinsk et al., 2007; Traykovski, 2007; Cummings et al., 2009; Yamaguchi and Sekiguchi, 2011). Coarse grained ripples have been observed in shelf environments for several decades (e.g., Forbes and Boyd, 1987; Leckie et al., 1988 and references therein) but until recently ripple measurements have not been coupled to the hydrodynamic parameters of their formation. Recent lab work by Cummings et al., (2009) demonstrated the persistence of steep ripples with orbital scaling in coarse sand under strong hydrodynamic conditions.

These two new populations of ripples highlight a perennial problem with empirical predictors; unless equations are built using large, integrated data sets that encompass many conditions, prediction schemes are difficult to translate to different settings. A non-empirical approach, such as models based on first principles (e.g., Foti and Blondeaux, 1995; Blondeaux, 2001; Charru and Hinch, 2006), presents different problems: nonlinear, emergent processes that occur at the ripple scale such as flow separation, vortex ejection, turbulence, sediment suspension, pattern coarsening, defect creation, migration and annihilation (Werner and Kocurek, 1999), and the existence of multiple stable configurations in ripple sizes/shapes at a given hydrodynamic condition (a stability balloon; Hansen et al., 2001) limit the usefulness of finite-amplitude predictions. Prediction by numerical models of coupled fluid flow and bed evolution present promising results but have so far been tested under a narrow range of conditions and compared to few data sets (Marieu et al., 2008; Chou and Fringer, 2010).

If empirical data driven predictors are currently the most broadly applicable tools to develop field scale predictions, how should they be built? Traditionally the development of an empirical predictor relies on transforming a single (or several) noisy multidimensional dataset to lower-dimensions and fitting a curve (with a set functional form) through the resultant point cloud. Here we offer a different solution: a data integration campaign (the collection of many published datasets) followed by machine learning (ML), whereby computational optimization techniques are used to find solutions to multidimensional and nonlinear problems. The suite of techniques encompassed by ML are essentially identical to empirical data driven techniques used previously except the trial and optimization of solutions is outsourced to a computer.

The most common ML paradigm used in coastal studies is artificial neural networks (ANN). Recent examples of its use include predictions of alongshore sediment transport in the surfzone (van Maanen et al., 2010), sand bar behavior (Pape et al., 2010) and suspended sediment reference concentration under waves (Oehler et al., 2012). Yan et al. (2008) used an artificial neural network to predict wave ripple geometry (length and height) based on three input parameters (median grain size, wave period, and the maximum near bed wave orbital velocity). ANN results give better predictions based on 3 statistical measures (scatter index, correlation coefficient, and mean geometric deviation) than four common empirical models (Nielsen, 1981; Van Rijn, 1993; Wiberg and Harris, 1994; Grasmeijer and Kleinhans, 2004). Yet the ANN ripple prediction scheme derived by Yan et al. (2008) was developed and compared to a limited dataset. Furthermore ANNs are problematic because the highly nonlinear result is difficult to interpret and does not offer immediate insight into the physical nature of the problem at hand. Decision or regression trees (e.g., Oehler et al., 2012), another common and well performing ML technique, is also hampered by the lack of direct physical significance and other drawbacks such as the lack of smoothness.

In this contribution we use genetic programming (GP; Koza, 1992), a population based optimization technique where the population consists of individual equations (i.e. a population of individual predictors). The mathematical or logical operations that constitute each algorithms can be modified at every time step via an 'evolutionary' process (such as crossover and mutation) to produce expressions that optimize model-data fit. Outputs developed by GP can be smooth functions that are easy to examine and interpret for physical significance. Furthermore, *a priori* determination of the functional form of the predictor is not required and the final optimized solution can take on any mathematical form (within user defined limits). Thus far genetic programming has been applied to a wide range of problems including the prediction of freshwater phytoplankton dynamics (Whigam and Recknagel, 1999), downscaling of atmospheric model output (Coulibaly, 2004), determining appropriate parameterization for roughness in vegetated flows (Baptist et al., 2007), wave forecasting (Kambekar and Deo, 2012) and mapping of seafloor habitats (Silva and Tseng, 2008).

The goal of this study is to demonstrate the applicability of ML techniques (specifically GP) to research questions in the coastal domain. To accomplish this goal we compile 27 different field and laboratory data sets of wave ripple prediction (995 individual measurements; Table 1) that span a broad range of conditions and develop a new wave-ripple predictor that is able to capture the morphology of ripple geometry in a wide range of forcing conditions, including conditions where long wave orbital ripples are present. We put our results in the context of existing formulations and theories, and assess the physical relevance of GP predictors. Our new equilibrium predictor ignores the effect of ripple orientation, time evolution, heterogeneous sediment, superimposed current, ripple asymmetry, and bio-degradation of ripples. We discuss these limitations in the discussion section but note here that other existing time dependent ripple prediction schemes capture one or more (but not all) of these processes (i.e., Soulsby et al., 2012; Traykovski 2007). Finally, the compilation of published ripple data allows for the identification of gaps in knowledge and observations that should be pursued in future research. Future data collection campaigns can be added to this database, allowing for modifications to the prediction schemes shown below. In this sense the ripple prediction scheme we demonstrate here is dynamic.

2. Data

As a result of decades of study, many wave ripple datasets are available in the scientific literature. Examples of recent wave ripple data integration and compilations are Soulsby and Whitehouse (2005), Pedocchi and García (2009a) and Camenen (2009). Here we follow the lead of Pedocchi and García (2009a) and limit our data collection to studies using sediment with quartz (or near quartz) densities (2.65 g/cm^3) performed in large oscillatory tunnels, large wave flumes, wave racetracks and field conditions (i.e. we omit oscillating trays). Data on rolling-grain ripples, small bedforms that initially appear when flat beds are subject to oscillatory water motion, are ignored in this study because they have been experimentally shown to be a transient stage of ripple evolution (Faraci and Foti, 2001). We use 27 published studies in our dataset. Each measurement contains wave ripple, hydrodynamic, and sedimentological parameters. The dataset is split 59% / 41% between laboratory and field conditions (Table 1), and laboratory measurements are obtained from a 49% / 49% / 2% split between oscillatory tunnels, wave flumes, and wave racetracks. Measurement error is different for each data set in our database, a natural consequence of data integration campaigns that assemble data collected by different instruments and techniques. We assume that measurements of ripple data obtained in field settings are at or near equilibrium.

Our database can be visualized as a series of histograms showing the parameter range in our dataset (Figure 2). A majority of ripple measurements in our database occur at hydrodynamic conditions of $d_0 < 2$ m, $U < 0.75$ m/s and sedimentological conditions of $D_{50} < 0.5$ mm. Another notable attribute is the strong bimodal signature of ripple steepness centered at values of ~0.15 and ~0.01. These clusters represent steep ripples and 'hummocky' ripples, respectively. We base our prediction of wave ripple wavelength λ (m), ripple height η (m), and ripple steepness ϑ (η/λ; dimensionless) on four variables: wave period T (s), bottom orbital excursion d_0 (m), median grain size D_{50} (m), and maximum near bed orbital velocity U (m/s). A hallmark of field data sets is the irregular forcing, requiring us to reconcile different measured parameters. Several field datasets used in the compiled dataset reported hydrodynamic parameters in terms of significant values (U_{sig}, $d_{0,sig}$, and T_{sig}). We followed the protocol of Pedocchi and García (2009) and assume $U = U_{sig}$ (and furthermore $d_0 = d_{0,sig}$ and $T=T_{sig}$). We acknowledge that the merging of disparate data sources introduces uncertainty into the data.

The hydrodynamic and sedimentological conditions covered by this dataset can be visualized using 6 projections of the 4 dimensional phase space (Figure 3). Notable sparseness occurs in this database at strong hydrodynamic conditions, and at median seabed grain sizes above 0.5 mm. We use T, d_0, and U as separate independent variables for input to the GP (though they are related by $d_0=UT/\pi$) in an attempt to introduce no additional information about which of these parameters is most relevant. As GP is a data driven technique, the raw hydrodynamic data is given as input and the ML process determines which hydrodynamic variable(s) is most relevant from a statistical standpoint. We use T, d_0, D_{50}, and U to predict λ. Predicted λ is incorporated into the suite of variables (i.e., T, d_0, D_{50}, U) used to predict η. We combining the predictors for λ and η enable the development of a predictor for ripple steepness. Yet we do not enforce the accurate depiction of steepness in the development of ripple height and length predictors and imprecision in the λ and η equations may cause imprecision in the prediction of ϑ. However, in some circumstances accurate depiction of height and steepness is required for the parameterization of relevant processes (e.g. vertical suspended sediment diffusivity; Nielsen, 1992): therefore we also develop an independent ripple steepness predictor using the genetic programming technique. The development of a third predictor also further demonstrates the strengths and weaknesses of GP and ML techniques. Predicted λ and η are added to the variables (T, d_0, D_{50}, U) used to predict ϑ. The development of predictors for λ, η and ϑ without enforcing interoperability relies on users to decide which predictors are most important for the specific research question.

Several published studies measure two superimposed ripple scales (larger orbital scale ripples and smaller anorbital scale ripples) at a single hydrodynamic condition (e.g. Hanes et al., 2001; Pedocchi and García 2009b; Cummings et al., 2009). Work by Cummings et al., (2009) shows that both pattern modes occur as maximum orbital velocity is increased and the ripple pattern transitions from small scale (anorbital) ripples to large scale orbital ripples (‘hummocks’). Upon further velocity increase, the small scale ripples are destroyed and only the large scale orbital features remain (Cummings et al., 2009). The threshold of large scale orbital ripple appearance can be estimated from the work of Pedocchi and García (2009a) who found that large scale features appear at a threshold value of $U/w_s \cong 25$. When both anorbital and large scale ripples are present in tabulated data (e.g. Hanes et al 2001) we only include large scale ripples: the scaling of long wave ripples with bottom orbital diameter suggests a physical relationship to small scale orbital and suborbital ripples. In contrast, anorbital ripples scale with grain size (similar to current ripples) and the mechanism responsible for their formation may be different (Wiberg and Harris, 1994). We remove small-scale (anorbital) ripples from our database if they are present at values of $U_0/w_s \geq 25$; laboratory work by Cummings et al., (2009) and Pedocchi and García (2009a) suggests that this regime is dominated by large scale ripples. The targeted collection of field and laboratory data is needed to refine this threshold.

3. Methods

3.1 Selection of training, validation, and testing data

The database is split into three subsets to be used as training, validation, and testing. The GP algorithm uses the training dataset to develop and optimize candidate solutions. The validation dataset is used to evaluate the fitness of GP derived solutions and define which predictors persist. Testing data is not used or seen by the GP algorithm and is instead reserved as an independent test of the final predictors (and other published predictors). In the genetic programming literature there remains no proven 'best practice' for percentage of training, validation, and testing data, nor a well defined method of splitting these datasets. This may be because data splitting (e.g., the retention of a testing dataset) is not addressed in the foundational literature of the technique (as noted by Kushchu, 2002). Yet because our database of ripple measurements contains only sparse data at energetic hydrodynamic conditions and large grain sizes, the selection and partitioning of data into these three categories is crucial to develop a well performing predictor applicable to a range of environments (Bowden et al., 2002). For example, random division of the data has the potential to produce a significant problem; the training data is likely to misrepresent the full phase space of the entire dataset (i.e. exclude coarse grained and/or strong hydrodynamic data).

Informed data selection (i.e., selection based on clustering) has been shown to produce better results with ML predictors than 'blind' or random data selection (e.g., Bowden et al., 2002; May et al 2010). In this study we select training data through the use of a maximum dissimilarity algorithm (MDA; e.g., Camus et al., 2011). This algorithm is not a clustering routine (where cluster centroids are selected to represent a representative value of the data in the cluster), but instead a selection routine (where a centroid represents the most dissimilar data point from the previous centroids; Camus et al., 2011). Though our selection technique is different than the clustering techniques used by Bowden et al. (2002), our approach leads to a similar result: the use of a minimum of training data that is able to capture the variance in hydrodynamic and sedimentological conditions of the entire dataset while leaving more data to be used as validation and testing.

Our implemented version of the maximum dissimilarity algorithm is based on the description provided in Camus et al. (2011). Selection starts with the normalization of the data to a value between 0 and 1:

$$X_n = \frac{X - X_{min}}{X_{max} - X_{min}} \quad (1)$$

where X_n is the new normalized data value (between 0 and 1), X is the original value, X_{min} and X_{max} are the minimum and maximum of all values of variable X, respectively. After this normalization a single data point, a 'seed', is selected as the first centroid. Since our dataset is typified by sparseness in the coarse grain data, we use the largest grain size measurements as the first centroid (the 'seed'). The user selects the number of centroids and the algorithm then selects the additional centroids through an iterative process: Each data point in our data set is a 4-dimensional vector (normalized T, U, d_0, D_{50} space) and is associated with a distance to the nearest centroid. The single data point with the maximum distance between itself and the nearest centroid is selected as the next centroid (Camus et al., 2011). This routine continues until the user defined number of centroids is reached, after which data is denormalized.

There remains significant ambiguity in determining the appropriate number of centroids (or clusters) needed to accurately represent data, especially continuous data (e.g. May et al 2010). Our dataset on wave ripples is multidimensional and relatively continuous (i.e. not naturally clustered). Furthermore the dataset is sparse in areas because of a lack of collected data, while densely populated with measurements in other regions of phase space (e.g., experimental campaigns at specific hydrodynamic and/or sedimentological conditions). Since we intend to use selected centroids as representatives of the entire dataset, selecting too many centroids will likely rob the validation and testing datasets of poorly represented data (e.g., large T, U, d_0, D_{50}) while too few centroids will leave the testing data with to few data to capture the variability in the dataset. We use 30 centroids for the prediction of λ and 40 centroids for the prediction of η. Centroids used to represent η are also used for analysis of ϑ. Centroid locations can be seen in Figure 4. The use of fewer centroids (10-20) produced too few predictors while more centroids (~100) tended to produce many more nonlinear and potentially overfit solutions. In addition, the solutions obtained with more centroids were qualitatively similar to the solutions presented below using only 30-40 centroids. More centroids are used to predict ripple height because η is more difficult to predict (see also Yan et al., 2008; Williams et al., 2004). This is likely a result of the nonlinearities associated with ripple crests protruding into regions of flow with higher velocities: ripple height is likely more strongly influenced by suspension processes as a result. Data selected as the centroid locations are used for the training data. The points not selected as centroids (i.e. not selected as training data) are used for validation and testing data. Data is split between validation and testing randomly, without using a selection routine. Therefore the breakdown for the λ datasets is ~3% training, ~48% validation, ~48% testing, while the η (and ϑ) dataset breakdown is ~5% training, ~47% validation, ~47% testing.

3.2 Genetic programming

We operate on this compiled ripple data using the evolutionary computation technique of genetic programming (GP), a ML paradigm whereby candidate solutions (in the form of randomly generated equations) are evaluated and subsequently modified (Koza, 1992; Poli et al., 2008). The modification of candidate solutions is manifest as changes in variables and mathematical relationships between variables (i.e. the mathematical form), hence the description of this style of problem as 'symbolic regression'. Variables used in this study to predict wave ripple geometry are T, U, d_0,

D_{50}, λ (for height and steepness prediction), η (for steepness prediction), as well as GP derived constants. Nondimensional, renormalized input (from 0-1) is not necessary with GP (as it is with other ML techniques), and input is fed into the algorithm with units. Only D_{50} is renormalized in this analysis, and fed into the GP in units of mm (as opposed to m, but the presentation of all results in this contribution are in meters). Mathematical operators used in this study are $+$ (addition), $-$ (subtraction), $\times$ (multiplication), $\div$ (division), √ (square root), as well as integer powers ($e.g.\ \ x^2, x^3, x^4$). Furthermore we omit logical functions (e.g. if-then-else) because of the lack of smoothness when incorporating these components.

Candidate solutions are evaluated based a ‘fitness function’, a user defined error metric that determines how well a given candidate fits the validation data. Mean squared error (MSE) is used as the fitness function:

$$MSE = \frac{(p-b)^2}{n} \qquad (2)$$

where MSE is the Mean Squared Error, n is the sample size, p are the predicted values, and b are the observed values. The correlation coefficient, one of the error metrics used in previous ripple studies (Yan et al., 2008), was not used as a fitness function because it tended to develop nonphysical predictors (negative wavelengths and heights under certain conditions) that matched the shape of the data but did not align well with actual magnitudes.

Equations that minimize mean squared error are retained, while poor performing solutions are discarded. Retained solutions are combined, rearranged and manipulated in a probabilistic manner according to evolutionary processes; solutions 'crossover' by combining elements of other solutions to develop a new solution and 'mutations' develop new mathematical expression to substitute or tack on to a previous solution. As an example, candidate solutions are commonly encoded in GP software as ‘trees’, and the modification of candidate solutions (change of variables and/or mathematical expression) is accomplished through adjustments in tree ‘limbs’ (Figure 5). Through time predictors gain complexity (i.e. trees grow in size) as they are recombined in a variety of ways, moving from simple equations (e.g. two variables and one mathematical symbol linking them) to highly nonlinear, complex expressions (e.g. many variables linked by many symbols). In this way the growth and adjustment of candidate solutions enables the searching of an increasingly larger phase space (i.e. variable and symbolic space), and find optimized solutions to the problem at hand. This search process occurs until a solution with zero error is found or the routine is terminated.

In this study we use a proven symbolic regression/genetic programming software package developed by Schmidt and Lipson (2009; 2013). This software package, ‘Eureqa’, modifies the tree-based encoding outlined above by eliminating redundancy when multiple ‘tree limbs’ are identical. The software output is a suite of solutions with increasing mathematical ‘complexity’, where complexity is a count of the numbers of operations and variables used in the candidate solution. Each solution of a given complexity represents the equation with the least error compared to identically ‘complex’ candidate solutions. Furthermore, to be retained in the solution set, a given solutions must have less error compared to all previous less-complex solutions. Therefore the suite of solutions that is developed as output lie along the ‘Pareto front’, a line in complexity-fitness space that illustrates fitness increases with the increasing complexity of candidate solutions. Because simple predictors are retained though more complex predictors may fit the data with less error, the user must pick a single solution as the final predictor of choice.

3.3 Generalization and overfitting

The lack of a single optimal solution as output from the GP algorithm is likely a consequence of using noisy data (e.g., field data) and examining a phenomena that may not have a single solution, but instead a small range of possible solutions (i.e., there may be multiple stable ripple configurations for a given hydrodynamic/sedimentological condition, a 'stability balloon'; Hansen et al., 2001). The determination of an ideal solution from the GP program was further complicated because there is no stoppage routine built into the algorithm (e.g., based on fitness) used in this study. We cease the search after roughly 10^{10} formulas have been evaluated as continued search shows only marginal increases in predictive power (and this increase occurs only on more complex, likely overfit, predictors). The solutions were then evaluated to determine the most appropriate final predictor. Several methods for eliminating overfit solutions exist (e.g., Gonçalves et al., 2012). We use several techniques in parallel to determine appropriate solutions: 1) bias toward shorter, physically reasonable solutions, 2) examining 'cliffs' in the Pareto front, and 3) examination of solution fit.

Many of the more complex solutions have lower error with training and validation data but are physically uninterpretable. Therefore when evaluating the family of solutions from a given genetic programming iteration we tend to bias our search for the most universal predictor by preferring compact solutions because they tend to offer more generalization and are likely less overfit (The minimum description length principle; e.g., O'Neill et al., 2010). Shorter solutions reappear with repeat initialization of the genetic programming algorithm, suggesting that these represent the globally optimum solutions for a given function size. Longer solutions do not tend to reappear, either a result of a large search space that is not repeated during repeat initializations or the presence of multiple, equally optimal solutions in the large phase space (i.e. local minima). The inherent reproducibility of simple, weakly nonlinear solutions suggests their use as predictors until further data can be used to justify the use of highly nonlinear predictors.

Aside from examining the solutions from least complex to most complex, examining areas along the Pareto front where large gains in prediction are obtained with small gains in solution complexity is a natural place to observe potential solutions (Figure 6). These areas along the Pareto front are referred to as 'cliffs'. Schmidt and Lipson (2009) used the last of such 'cliffs' to observe many physically relevant solutions. In this study final solutions were chosen from the subset of solutions that are 'cliffs' along the Pareto front

Candidate solutions are evaluated by minimizing error functions. Occasionally candidate solutions are able to minimize the mean squared error but provide unphysical solutions (e.g. negative ripple wavelengths under some conditions) or generally poor global performance (e.g. flat, constant predictors). These solutions must be manually disregarded, as there is as yet no means of excluding them.

3.4 Comparison with other predictors

Predictor performance is evaluated, using the independent testing data, with the Normalized Root Mean Squared Error (NRMSE):

$$NRMSE = \frac{\sqrt{MSE}}{\bar{b}} \qquad (3)$$

where $\bar{b}$ is the mean of the observed values. Additionally we report correlation coefficient (Pearson's *r*) for each predictor evaluated against the independent testing data.

We compare our results to two recently developed and widely used predictors: Soulsby and Whitehouse (2005; also reported in Soulsby et al., 2012) and Pedocchi and García (2009a). As noted by Soulsby et al., (2012), recent work by Camenen (2009) using a large compiled database of ripple measurements found the Soulsby and Whitehouse (2005) formulation to be the best overall predictor compared to those developed by Grant and Madsen (1982), Wikramanayake and Madsen (1991), Van Rijn (1993), Mogridge et al., (1994), Wiberg and Harris (1994), and Grasmeijer and Kleinhans (2004). The recent work of Pedocchi and García (2009a), which was not evaluated by Camenen (2009), yields good collapse of the data compared to other the predictors mentioned above and performs well in field conditions (Bolaños et al., 2012). The Soulsby and Whitehouse (2005) predictor for length and steepness (η/λ) is:

$$\frac{\lambda}{A} = \left[1 + (1.87\times10^{-3})\frac{A}{D_{50}}\left(1 - e^{\left\{-\left(2.0\times10^{-4}\frac{A}{D_{50}}\right)^{1.5}\right\}}\right)\right]^{-1} \qquad (4)$$

$$\frac{\eta}{\lambda} = 0.15\left[1 - e^{\left\{-\left(5000\frac{D_{50}}{A}\right)^{3.5}\right\}}\right] \qquad (5)$$

where A is the wave orbital amplitude ($2A=d_0$). Combining (4) and (5) yields η alone. The Pedocchi and García (2009a) predictor is:

$$\frac{\lambda}{d_0} = \begin{cases} 0.65\left[\left(0.050\dfrac{U}{w_s}\right)^2 + 1\right]^{-1}, & Re_p \geq 13 \\ 0.65\left[\left(0.040\dfrac{U}{w_s}\right)^2 + 1\right]^{-1}, & 9 \leq Re_p < 13 \\ 0.65\left[\left(0.054\dfrac{U}{w_s}\right)^3 + 1\right]^{-1}, & Re_p < 9 \end{cases} \qquad (6)$$

$$\frac{\eta}{d_0} = \begin{cases} 0.1\left[\left(0.055\dfrac{U}{w_s}\right)^3 + 1\right]^{-1}, & Re_p \geq 13 \\ 0.1\left[\left(0.055\dfrac{U}{w_s}\right)^4 + 1\right]^{-1}, & 9 \leq Re_p < 13 \\ 0.1\left[\left(0.055\dfrac{U}{w_s}\right)^5 + 1\right]^{-1}, & Re_p < 9 \end{cases} \qquad (7)$$

where w_s is evaluated for D_{50} and Re_p is a dimensionless particle size (Pedocchi and García, 2009a) evaluated as:

$$Re_p = \frac{\sqrt{gRD_{50}}D_{50}}{\nu} \qquad (8)$$

where g is gravity, R is the submerged specific density of sediment (here taken to be 1.65) and ν is kinematic viscosity. The three size classes ($Re_p \geq 13, 9 \leq Re_p < 13$ and $Re_p < 9$) correspond to coarse, medium and fine sand respectively and the three separate equations result in slight discontinuities.

Lastly we note that we are unable to compare the performance of our GP derived predictor to the ANN model developed by Yan et al., (2008) as we do not know the final optimized ANN equation developed by Yan et al., (2008). In addition, we do not know which data was used as training/validation or testing in the development of the ANN model.

4. Results

4.1 Ripple wavelength

The GP algorithm output is shown in Table 2. This experiment evaluated 10^{10} formulas to develop the Pareto front shown in Figure 6. Cliffs, significant gains in error for small changes in equation complexity occur along the Pareto front at complexities of 3, 6, and 8 (Figure 6) The first of these cliffs (at complexity 3) is a predictor, $\lambda = 0.607d_0$, that mimics the basic form of the orbital scale (i.e. weak hydrodynamics) predictor commonly used today, where ripple wavelength is a linear function of orbital excursion (e.g. $\lambda = 0.65d_0$ from Miller and Komar, 1980a; $\lambda = 0.62d_0$ from Wiberg and Harris, 1994). Debate surrounds the correct value of the coefficient modifying orbital excursion, especially in medium to coarse sand (e.g. Becker et al., 2007; Traykovski et al., 1999). All solutions that are more complex than the solution of complexity 3 demonstrate why there is debate: the coefficient is likely a function of grain size. We rule out solution 3 as a viable universal predictor because grain size is a control on ripple length (e.g., Cummings et al., 2009). We focus our remaining examination on the solution at complexity 8.

$$\lambda = \frac{d_0}{1.12 + 2.18(1000D_{50})} \qquad (9)$$

Figure 7 shows the general behavior of this predictor: increasing wave ripple spacing with increasing bottom orbital excursion and decreasing wave ripple wavelength with increasing grain size. Furthermore ripple length is more sensitive to median grain size at larger orbital diameter. Previous ripple length prediction schemes have focused on orbital diameter and grain size as they represent the two fundamental length scales in the development of oscillatory bedform. For instance, Soulsby and Whitehouse (2005) develop an equilibrium predictor where A/ D_{50} is the controlling parameter after examining the collapse of compiled data with several other variables.

Using only the reserved testing data, the NRMSE of the new GP predictor as well as those developed by Soulsby and Whitehouse (2005) and Pedocchi and García (2009a), are 0.74, 1.33, and 1.22 respectively, and the correlation coefficient is 0.78, 0.02, and 0.20 respectively. The GP derived predictor performs better than the other predictors based on the NRMSE and correlation coefficient. Figure 8 shows the performance of these models in both linear and log-log space. Neither of these previously published predictors were developed for large scale orbital ripples, and both show predictions that deviate significantly when observed ripple wavelengths are large. The GP derived predictor is better able to capture large scale ripples. Both Soulsby and Whitehouse (2005) and Pedocchi and García (2009a) are able to better capture small scale 'anorbital' ripples that deviate significantly from the scaling of (9).

4.2 Ripple height

The GP algorithm output is shown in Table 3. This experiment evaluated 10^{10} formulas to develop the Pareto front shown in Figure 9. Cliffs occur along the Pareto front at complexities of 3, 5, 14, 18 and 36 (Figure 9). Predictor of complexity 3, $\eta =0.435d_0$, is qualitatively similar to predictions of ripple height in the orbital regime (i.e. weak hydrodynamics) presented in Wiberg and Harris (1994), where ripple wavelength is a function of orbital diameter and ripple steepness (η/λ) is constant, therefore ripple height is a linear function of bottom orbital diameter. Constant steepness breaks down in stronger hydrodynamic conditions, and this is reflected in the inclusion of grain size and ripple length in more complex predictors. We have no compelling evidence to use the most nonlinear but best fit solution (36), nor is there compelling evidence at this time that ripple height has a such a strongly nonlinear dependence on grain size (Solution 14 and 18). We focus our analysis on solution 5:

$$\eta = 0.313\lambda(1000D_{50}) \qquad (10)$$

or, replacing λ (which denotes predicted ripple wavelength) with equation 9:

$$\eta = \frac{0.313d_0(1000D_{50})}{1.12 + 2.18(1000D_{50})} \qquad (11)$$

Figure 10 shows the behavior of this predictor under conditions of various orbital diameter and grain size. Ripple height increases with increasing grain size and orbital diameter. As with ripple length, ripple height is more sensitive to changes in grain size than changes in orbital velocity. Reserved testing data is used as an independent dataset to compare the GP predictor as well as those developed by Soulsby and Whitehouse (2005) and Pedocchi and García (2009a): the NRMSE for each predictor is 0.79, 1.02, and 1.01 respectively, and the correlation coefficient is 0.67, 0.41, and 0.47 respectively. The GP derived predictor performs better than the other predictors based on the NRMSE and correlation coefficient. Figure 11 shows the performance of these models in both linear and log-log space.

4.3 Ripple steepness:

Combining the GP predictors for ripple length (9) and height (11), or simply rearranging (10), yields a predictor for ripple steepness:

$$\vartheta = 0.313(1000D_{50}) \qquad (12)$$

implying that steepness is a function solely of grain size, which is a gross approximation of the variability observed in the data, and to some extent even unphysical. To enhance our steepness prediction we produce a GP derived steepness predictor. The GP algorithm output is shown in Table 4. This experiment evaluated 10^{10} formulas to develop the Pareto front shown in Figure 12. Cliffs, significant gains in error for small changes in complexity occur along the Pareto front at complexities 5, 8, 10, and 16. The predictor at complexity 5 produces nonphysical results (negative steepness under some conditions) so is ruled out. The most nonlinear predictor reported (complexity of 16) shows only small decrease in error for increasing equation complexity; we focus our analysis on predictor 10:

$$\vartheta = \frac{3.42}{22 + \left(\frac{\lambda}{(1000D_{50})}\right)^2} \qquad (13)$$

by replacing λ (predicted ripple wavelength) with (9), yields:

$$\vartheta = \frac{3.42}{22 + \left(\frac{d_0}{1.12(1000D_{50}) + 2.18(1000D_{50})^2}\right)^2} \qquad (14)$$

Figure 13 shows the behavior of this predictor under conditions of various orbital diameter and grain size. Increasing D_{50} (for a given d_0) results in increasing ϑ until a saturated value of 0.15 is reached. Increasing d_0 (for a given D_{50}) results in decreasing ϑ. Small grain sizes are very sensitive to changes in d_0, while large grain sizes are relatively insensitive. Figure 14 shows the performance of (14) against the independent testing data compared to the linear convolution of GP derived length and height (12), as well as the Pedocchi and García (2009a) and Soulsby and Whitehouse (2005) predictors. The

NRMSE of these predictors is: 0.36, 0.50, 0.47, and 0.43, respectively, and the correlation coefficient is 0.70, 0.48, 0.63, and 0.50 respectively. The GP derived predictor performs better than the other predictors (including the linear convolution of GP derived λ and η) based on the NRMSE and correlation coefficient.

5. Discussion

5.1 Predictors derived from genetic programming

The suite of predictors that are produced as output of the genetic programming show a trend of increasing predictability with increasing complexity. Highly nonlinear predictors have been avoided in this study because they may be fit to the noise or variance present in the training dataset (i.e. they are overfit). Yet the more complex nonlinear predictors can be used as hypothesis for further field and lab studies where grain size effects are a focus.

Dependence on orbital scaling and grain size is not imposed by the authors, it is a result of the data used to feed the genetic programming software. Aside from the data sets used in this study, other field observations have shown decreasing ripple height and increasing ripple length in fine grained sand under strong hydrodynamic forcing (e.g., a transition from steep to low profile bedforms; Green and Black, 1999; Green et al., 2004; Trembanis et al., 2004). Pedocchi and García (2009a) and Cummings et al. (2009) note that U is the major control on the transition from small ripples (anorbital) to large ripples (hummocks), yet our GP derived predictors contain only one hydrodynamic parameter, d_0. Furthermore dependence on U is not present in any of the candidate predictors (Tables 2,3, and 4). This is likely the result of several factors: First, d_0 and U are correlated in our database (Figure 3), making d_0 a potential proxy for any dependence on U. Second, our database likely contains multiple ripple sizes at similar hydrodynamic conditions, resulting in the lack of a clear velocity threshold. Third, we focus on developing a continuous predictor so do not include any logical statements that can accommodate a threshold.

Our results show that ripple height is more difficult to predict than ripple length (e.g., Yan et al 2008; Williams et al 2004). As mentioned previously, this is likely a consequence of ripple crests being subject to higher flow velocities and suspension processes. Yet successful height and steepness determination is important for the prediction of sediment transport, in particular the reference concentration (e.g., Green and Black 1999) and sediment diffusivity (e.g., Nielsen 1992, Thorne et al., 2009). Only 2 equations are needed to predict height, length and steepness of ripples, but error in the two chosen predicted parameters cascades to the third. The basic linear convolution of predicted λ (9) and predicted η (11) demonstrate this cascading error: the resultant steepness predictor (12) produces results that are solely dependent on grain size. We instead offer 3 separate equations in the hope that workers will decide which 2 predictors are most valuable for a specific research question. Notably, the GP algorithm did have predicted λ and predicted η available as equation building blocks when determining ripple steepness but the term 'η/λ' did not appear in any candidate solutions (Table 4). Generating 3 separate predictors that are not self-consistent leads to geometric inconsistencies, but results in better prediction for work that requires accurate prediction of height and steepness but does not rely on ripple length measurements.

The hydrodynamic and sedimentological limit of the current prediction scheme is represented by the 4-dimensional shape that outlines the point cloud in Figure 3 (Table 1 contains more information regarding the range of the dataset). We excluded conditions where ripples are not present either as a result of sheet flow conditions (upper plane bed) or because of insufficient mobility (lower plane bed). Uncertainty in the onset of upper plane bed exists because of the lack of data at a range of D_{50} in field-scale conditions (e.g., Li and Amos, 1999; Trembanis et al., 2004; You and Yin, 2006). Additionally, field work suggests that upper plane bed conditions may not be flat, but instead typified by dynamic features that may be similar if not identical to long wave ripples (Green and Black, 1999; Green et al., 2004; Trembanis et al., 2004). As a result of the ambiguity in bed state under 'upper plane bed' conditions we did not compare our predictor to the version developed by Camenen (2009), which explicitly includes a sheet flow threshold (where ripples are destroyed). Furthermore we do not compare the GP derived predictors with those developed by Williams et al., (2005), who developed separate predictors for short wavelength and long wavelength ripples. We intentionally did not divide our dataset (and develop separate predictors) in an attempt to construct a practical prediction scheme that spans a wide range of conditions. Since this study aims to produce a continuous predictor of wave ripple geometry, the use of discontinuous functions (logical statements: e.g. 'if-then-else') has not been explored quantitatively in this contribution. This study does not tackle the issue of time dependent adjustment of bedforms in unsteady flow (Austin et al., 2007, Soulsby et al., 2012, Traykovski 2007; Davis et al., 2004; Doucette and O'Donoghue, 2006; Hay 2008), the importance of initial conditions on final ripple configuration (Traykovski et al., 1999; Hansen et al., 2001), or the explicit incorporation of emergent ripple parameters (e.g., defect density; Skarke and Trembanis, 2011).

5.2 Open Research Questions: Wave Ripples

Data integration campaigns can highlight gaps in knowledge. The collection of new ripple datasets will be able to be used as either independent tests of the predictors developed in this study (if the setting corresponds to an area in figure 3 that is dense with points) or as new data to train the GP algorithm (if the data correspond to unexplored or sparse area in figure 3; Bowden et al., 2012). Additional datasets of wave ripple geometry that include more input parameters (e.g. measures of grain sorting, wave irregularity, initial conditions, time dependence) are needed if prediction accuracy is to increase. Furthermore datasets that encompass coarse grained environments (coarse sand and gravel) and datasets in energetic conditions are still needed. Though coarse grained conditions reflect a smaller fraction of the seabed than fine grained settings, coarse grained environments are likely important nursery habitat for fish (Hallenbeck et al., 2012). Collection of this data will not only help in the determination of ripple configuration under these specific forcing conditions, but linking these environments with the present data will allow for the development of a better predictor by defining the shape of the prediction surface over a greater extent in phase space.

Conditions with waves and currents (e.g., Lacy et al., 2007; Khelifa and Ouellet, 2000; Arnott and Southard, 1990) are excluded from this analysis. The collection and integration of data with waves and currents may lead to a more universal bedform predictor in the future but more data on ripple geometry under wave and current forcing is needed for machine learning techniques to be applied successfully. The dataset in this study uses median grain size as the sole sedimentological metric for predicting ripple geometry. Yet many field settings may not be accurately described by a sharp peaked unimodal distribution of grain sizes, and therefore prediction of ripples using D_{50} may lead to significant error. Foti and Blondeaux (1995) showed that the addition of coarse sediment can act as stabilizing feature, enhancing ripple length. It is possible that graded sediment will not conform to the predictive tools outlined above. But what is the effective D_{50} in graded sediment when predicting ripples? Furthermore variations in grain shape and bed porosity may also impact the geometry of ripples. More research is needed into the role of mixed grains in determining equilibrium wave ripple geometry (e.g. Calantoni et al., 2013).

More studies are needed to better constrain thresholds between short 'anorbital' ripples and large 'orbital' scale ripples (Pedocchi and García, 2009a, 2009b; Cummings et al., 2009; Maier and Hay, 2009). Experimental work has thus far shown that there exists no intermediate scale between these two configurations (Dumas et al., 2005; Cummings et al., 2009). The determination of when large ripples appear and when superimposed short ripples disappear will allow the pruning of the database in regions where overlapping ripple scales occur. The decision of which ripple scale to eliminate when both exist is a function of the research question being studied.

5.3 Open Research Questions: Data Driven Prediction

In this contribution we demonstrate a selection technique whereby very few data are used to train the GP algorithm and most data is used as validation and independent testing. The training data was selected solely from variables representing the forcing conditions. As a result the training data is not representative of the entire population of ripple configurations as data points that are neighbors in 'forcing space' do not necessarily have similar ripple geometries. The selected training data is therefore only related to the range of forcing present in the dataset, not the range of ripple geometry. Therefore we believe that our sampling strategy does not bias the testing of the predictors (which relies on ripple geometry) using the reserved, unselected testing data.

We define the testing dataset as ‘independent’ because it was not shown to the GP algorithm. Additionally we performed experiments by removing several individual datasets from the composite dataset. The removed data serves as testing data that is not shown to the selection routine, not shown to the GP algorithm, and additionally not related to data shown to the selection routine/GP (this is another definition of ‘independent’). The resultant predictors (not shown) were quantitatively similar to those presented in this contribution and similarly performed better than the Pedocchi and García (2009a) and Soulsby and Whitehouse (2005) predictors using only the smaller sample of removed datasets as testing. Is it enough for testing data to be unseen by the ML algorithm, or do entire datasets need to be reserved whole as testing data? More investigation will resolve this issue.

Even though we were able to obtain good results using few centroids, we are unaware of a technique for quantitatively determining the optimal number of centroids to capture the variability in the data set while leaving the maximum amount of data for use as validation/testing. Furthermore many selection and clustering routines are available, and it is unclear which routine is optimal for a given dataset. It is likely that some of the answers to these questions lie in statistical science and computer science literature that has not fully percolated into the Earth Sciences.

Our observations with the GP software show too few centroids tend to underfit the data because the GP has too little training data to develop applicable solutions. With few training data solutions tend to be linear and have low RMSE when compared tot the validation and testing datasets. Training datasets that are larger than used in this study (> 40 centroids) tend to produce more large (complexity > 30) nonlinear solutions. In addition, the solutions at complexity less than 30 are similar (if not identical) to the solutions in this study (using smaller training datasets). The invariance of solutions gives qualitative justification to the number of centroids used in this study, but we do not offer a quantitative technique for determining the minimum number of training data needed to capture dataset variability. Furthermore how is this number linked to the quantity and quality of the data in the training dataset? Lastly, the stability and final criterion for selecting a single predictor is subjective and can likely be improved or quantitatively justified by implementing more sophisticated accounting techniques based on information such as the Aikake Information Criterion (AIC) or the Bayesian Information Criterion (BIC).

6. Conclusion

We develop equilibrium predictors of oscillatory ripple geometry using genetic programming. Ripple length is a weak nonlinear function grain size and bottom orbital excursion. Ripple height and steepness are nonlinear functions of grain size and predicted ripple length (i.e. grain size and bottom orbital excursion). Furthermore these new predictor encompass a wide range of hydrodynamic and sedimentological conditions not previously included in published prediction schemes. However, the proposed method is not suitable for practical applications with significant currents present, nor under conditions that would either be below the threshold of motion or above the threshold of ripple wash-out. Such conditions should be identified separately by existing methods (Nielsen, 1992; Lacy et al., 2007; Camenen, 2009; Soulsby et al., 2012)

This contribution further demonstrates the viability of developing empirical predictors through ML techniques. As previously mentioned by Oehler et al., (2012), ML algorithms could be integrated into future morphodynamics models (model-data fusion and the development of a 'hybrid' model; Krasnapolsky and Fox-Rabinovitz, 2006), replacing functions with large uncertainty.

The data integration campaign (which preceded the implementation of the GP algorithm) had the side benefit of highlighting the current state of our knowledge on ripple geometry, potentially motivating targeted data collection campaigns. Newly collected data can be fed back into the GP software to develop revised predictors.

Acknowledgments: We thank Paula Camus for sharing her MDA routine, Malcolm Green for insightful comments at the beginning of this study, and three anonymous reviewers for critical feedback. EBG thanks 'IH Cantabria' for funding during his stay, where part of this work was completed. G.C. acknowledges funding from the "Cantabria Campus Internacional, Augusto Gonzalez Linares Program".

References

Ardhuin, F., Drake, T.G., Herbers, T.H.C., 2002. Observations of wave-generated vortex ripples on the North Carolina continental shelf. Journal of Geophysical Research 107(C10), 3143, doi:10.1029/2001JC000986.

Arnott, R.W., Southard, J.B., 1990. Exploratory flow-duct experiments on combined-flow bed configurations, and some implications for interpreting storm-event stratification. Journal of Sedimentary Research 60(2), 211-219.

Austin, M.J., Masselink, G., O'Hare, T.J., Russell, P.E., 2007. Relaxation time effects of wave ripples on tidal beaches. Geophysical Research Letters 34, L16606, doi:10.1029/2007GL030696.

Baptist, M.J., Babovic, V., Uthurburu, J.R., Keijzer, M., Uittenbogaard, R.E., Mynett, A., Verwey, A., 2007. On inducing equations for vegetation resistance. Journal of Hydraulic Research 45, 435-450.

Becker, J.M., Firing, Y.L., Aucan, J., Holman, R., Merrifield, M., Pawlak, G., 2007. Video-based observations of nearshore sand ripples and ripple migration. Journal of Geophysical Research 112, C01007, doi:10.1029/2005JC003451. .

Blondeaux, P., 2001. Mechanics of coastal forms. Annual Review of Fluid Mechanics 33, 339-370.

Bolaños, R., Thorne, P.D., Wolf, J., 2012. Comparison of measurements and models of bed stress, bedforms and suspended sediments under combined currents and waves. Coastal Engineering 62, 19-30.

Bowden, G.J., Maier, H.R., Dandy, G.C., 2002. Optimal division of data for neural network models in water resources applications. Water Resources Research 38(2), doi:10.1029/2001WR000266 .

Bowden, G.J., Maier, H.R., Dandy, G.C., 2012. Real-time deployment of artificial neural network forecasting models: Understanding the range of applicability. Water Resources Research 48 W10549, doi:10.1029/2012WR011984.

Boyd, R., Forbes, D.L., Heffler, D.E., 1988. Time-sequence observations of wave-formed sand ripples on an ocean shoreface. Sedimentology 35, 449-464.

Calantoni, J., Landry, B.J. and Penko, A.M., 2013. Laboratory observations of sand ripple evolution using bimodal grain size distributions under asymmetric oscillatory flows In: Conley, D.C., Masselink, G., Russell, P.E. and O'Hare, T.J. (eds.), Proceedings 12th International Coastal Symposium (Plymouth, England), Journal of Coastal Research, Special Issue No. 65, pp. 1497-1502, ISSN 0749-0208.

Camenen, B., 2009. Estimation of the wave-related ripple characteristics and induced bed shear stress. Estuarine, Coastal and Shelf Science 84, 553-564.

Camus, P., Mendez, F.J., Medina, R., Cofiño, A.S., 2011. Analysis of clustering and selection algorithms for the study of multivariate wave climate. Coastal Engineering 58, 453-462.

Chang, Y.S., Hanes, D.M., 2004. Suspended sediment and hydrodynamics above mildly sloped long wave ripples. Journal of Geophysical Research 109, C07022, doi:10.1029/2003JC001900.

Charru, F., Hinch, E.J., 2006. Ripple formation on a particle bed sheared by a viscous liquid. Part 2. Oscillating flow. Journal of Fluid Mechanics 550, 123-137.

Chou, Y.J., Fringer, O.B., 2010. A model for the simulation of coupled flow-bed form evolution in turbulent flows. Journal of Geophysical Research 115, C10041, doi:10.1029/2010JC006103.

Clifton, H.E., 1976. Wave-formed sedimentary structures: A conceptual model, in Beach and Nearshore Sedimentation, Spec. Publ. 24, edited by R. A. Davis Jr. and R. L. Ethington, pp. 126–148, Soc. for Sediment. Geol., Tulsa, Okla.

Coulibaly, P., 2004. Downscaling daily extreme temperatures with genetic programming. Geophysical Research Letters 31, L16203, doi:10.1029/2004GL020075.

Cummings, D.I., Dumas, S., Dalrymple, R.W., 2009. Fine-grained versus coarse-grained wave ripples generated experimentally under large-scale oscillatory flow. Journal of Sedimentary Research 79, 83-93.

Davis, J.P., Walker, D.J., Townsend, M., Young, I.R., 2004. Wave-formed sediment ripples: Transient analysis of ripple spectral development. Journal of Geophysical Research 109, C07020, doi:10.1029/2004JC002307 .

Delgado Blanco, M., Bell, P., Montaliu, J., 2004. A new look to the applicability of classical models for ripple prediction. In: Proc. 29th Int. Conf. Coastal Eng. ASCE, Lisbon, Portugal, pp. 1909–1921.

Doucette, J.S., 2000. The distribution of nearshore bedforms and effects on sand suspension on low-energy, micro-tidal beaches in Southwestern Australia. Marine Geology 165, 41-61.

Doucette, J.S., 2002. Geometry and grain-size sorting of ripples on low-energy sandy beaches: field observations and model predictions. Sedimentology 49, 483-503.

Doucette, J.S., O'Donoghue, T., 2006. Response of sand ripples to change in oscillatory flow. Sedimentology 53, 581-596.

Dumas, S., Arnott, R.W.C., Southard, J.B., 2005. Experiments on oscillatory-flow and combined-flow bed forms: implications for interpreting parts of the shallow-marine sedimentary record. Journal of Sedimentary Research 75, 501-513.

Faraci, C., Foti, E., 2001. Evolution of small scale regular patterns generated by waves propagating over a sandy bottom. Physics of Fluids 13, 1624-1634.

Faraci, C., Foti, E., 2002. Geometry, migration and evolution of small-scale bedforms generated by regular and irregular waves. Coastal Engineering 47, 35-52.

Forbes, D.L., Boyd, R., 1987. Gravel ripples on the inner Scotian Shelf. Journal of Sedimentary Research 57(1) 46-54.

Foti, E., Blondeaux, P., 1995. Sea ripple formation: the heterogeneous sediment case. Coastal Engineering 25, 237-253.

Gonçalves, I., Silva, S., Melo, J., Carreiras, J., 2012. Random sampling technique for overfitting control in genetic programming. Genetic Programming. In: Moraglio, A., Silva, S., Krawiec, K., Machado, P., Cotta, C. (eds.) EuroGP 2012. LNCS, vol. 7244, pp. 218–229. Springer, Heidelberg .

Grant, W.D., Madsen, O.S., 1982. Movable bed roughness in unsteady oscillatory flow. Journal of Geophysical Research 87, 469-481.

Grasmeijer, B.T., Kleinhans, M.G., 2004. Observed and predicted bed forms and their effect on suspended sand concentrations. Coastal Engineering 51, 351-371.

Green, M.O., Black, K.P., 1999. Suspended-sediment reference concentration under waves: field observations and critical analysis of two predictive models. Coastal Engineering 38, 115-141.

Green, M.O., Vincent, C.E., Trembanis, A.C., 2004. Suspension of coarse and fine sand on a wave-dominated shoreface, with implications for the development of rippled scour depressions. Continental Shelf Research 24, 317-335.

Hallenbeck, T.R., Kvitek, R.G., Lindholm, J., 2012. Rippled scour depressions add ecologically significant heterogeneity to soft-bottom habitats on the continental shelf. Marine Ecology Progress Series 468: 119-133.

Hanes, D.M., Alymov, V., Chang, Y.S., Jette, C., 2001. Wave-formed sand ripples at Duck, North Carolina. J. Geophys. Res 106, 22575-22592.

Hansen, J.L., v. Hecke, M., Ellegaard, C., Andersen, K.H., Bohr, T., Haaning, A., Sams, T., 2001. Stability balloon for two-dimensional vortex ripple patterns. Physical Review Letters 87.

Hay, A.E., 2008. Near-bed turbulence and relict waveformed sand ripples: Observations from the inner shelf. Journal of Geophysical Research 113, C04040, doi:10.1029/2006JC004013.
Hume, T.M., Green, M.O., Oldman, J.W., 1999. What happens at the seabed off a headland during a tropical cyclone, Coastal Sediments '99, Am. Soc. of Civ. Eng., Reston, Va. pp. 1836-1851.
Inman, D.L., 1957. Wave-generated ripples in nearshore sands, Tech. Memo. 100, Dep. of the U. S. Army Corps of Eng., Washington, D. C.
Kambekar, A.R., Deo, M.C., 2012. Wave prediction using genetic programming and model trees. Journal of Coastal Research 28, 43-50.
Kennedy, J. F., Falcon, M., 1965. Wave generated sediment ripples, Rep. 86, Hydrodyn. Lab., Mass. Inst. of Technol., Cambridge.
Khelifa, A., Ouellet, Y., 2000. Prediction of sand ripple geometry under waves and currents. Journal of waterway, port, coastal, and ocean engineering 126, 14-22.
Koza, J.R., 1992. Genetic Programming, On the Programming of Computers by Means of Natural Selection. MIT Press, Cambridge, MA, USA.
Krasnopolsky, V.M., Fox-Rabinovitz, M.S., 2006. A new synergetic paradigm in environmental numerical modeling: Hybrid models combining deterministic and machine learning components. Ecological Modelling 191, 5-18.
Kushchu, I., 2002. An evaluation of evolutionary generalisation in genetic programming. Artificial Intelligence Review 18, 3-14.
Lacy, J.R., Rubin, D.M., Ikeda, H., Mokudai, K., Hanes, D.M., 2007. Bed forms created by simulated waves and currents in a large flume. Journal of Geophysical Research 112, C10018, doi:10.1029/2006JC003942.
Leckie, D., 1988. Wave-formed, coarse-grained ripples and their relationship to hummocky cross-stratification. Journal of Sedimentary Research 58.
Li, M.Z., Amos, C.L., 1999. Sheet flow and large wave ripples under combined waves and currents: field observations, model predictions and effects on boundary layer dynamics. Continental Shelf Research 19, 637-663.
Maier, I., Hay, A.E., 2009. Occurrence and orientation of anorbital ripples in near-shore sands. Journal of Geophysical Research 114, F04022, doi:10.1029/2008JF001126.
Marieu, V., Bonneton, P., Foster, D.L., Ardhuin, F., 2008. Modeling of vortex ripple morphodynamics. Journal of Geophysical Research 113, C09007.
Masselink, G., Austin, M.J., O'Hare, T.J., Russell, P.E., 2007. Geometry and dynamics of wave ripples in the nearshore zone of a coarse sandy beach. Journal of Geophysical Research 112, C10022, doi:10.1029/2006JC003839.
May, R.J., Maier, H.R., Dandy, G.C., 2010. Data splitting for artificial neural networks using SOM-based stratified sampling. Neural Networks 23, 283-294.
Miller, M.C., Komar, P.D., 1980a. A field investigation of the relationship between oscillation ripple spacing and the near-bottom water orbital motions. Journal of Sedimentary Research 50(1) 173-182.
Miller, M.C., Komar, P.D., 1980b. Oscillation sand ripples generated by laboratory apparatus. Journal of Sedimentary Research 50(1) 183-191.
Mogridge, G.R., 1972. Wave generated bed forms, Ph.D. thesis, Queens Univ., Kingston, Ont., Canada.
Mogridge, G.R., Davies, M.H., Willis, D.H., 1994. Geometry prediction for wave-

generated bedforms. Coastal Engineering 22, 255-286.

Nielsen, P., 1981. Dynamics and geometry of wave-generated ripples. Journal of Geophysical Research 86, 6467-6472.

Nielsen, P., 1992. Coastal bottom boundary layers and sediment transport. World Scientific Publishing Company Incorporated.

O'Donoghue, T., Clubb, G.S., 2001. Sand ripples generated by regular oscillatory flow. Coastal Engineering 44, 101-115.

O'Donoghue, T., Doucette, J.S., Van der Werf, J.J., Ribberink, J.S., 2006. The dimensions of sand ripples in full-scale oscillatory flows. Coastal Engineering 53, 997-1012.

O'Neill, M., Vanneschi, L., Gustafson, S., Banzhaf, W., 2010. Open issues in genetic programming. Genetic Programming and Evolvable Machines 11, 339-363.

Oehler, F., Coco, G., Green, M.O., Bryan, K.R., 2012. A data-driven approach to predict suspended-sediment reference concentration under non-breaking waves. Continental Shelf Research 46, 96-106.

Pape, L., Kuriyama, Y., Ruessink, B.G., 2010. Models and scales for cross-shore sandbar migration. Journal of Geophysical Research 115, F03043.

Pedocchi, F., García, M.H., 2009a. Ripple morphology under oscillatory flow: 1. Prediction. Journal of Geophysical Research 114, C12014, doi:10.1029/2009JC005354.

Pedocchi, F., García, M.H., 2009b. Ripple morphology under oscillatory flow: 2. Experiments. Journal of Geophysical Research 114, C12015, doi:10.1029/2009JC005356.

Poli, R., Langdon, W.B., McPhee, N.F., 2008. A field guide to genetic programming. Lulu Enterprises Uk Limited.

Ribberink, J.S., Al-Salem, A.A., 1994. Sediment transport in oscillatory boundary layers in cases of rippled beds and sheet flow. Journal of Geophysical Research 99, 12707-12712.

Schmidt, M., Lipson, H., 2009. Distilling free-form natural laws from experimental data. Science 324, 81-85.

Schmidt, M., Lipson, H., 2013. Eureqa (Version 0.98 beta) [Software]. Available from http://www.eureqa.com/

Silva, S., Tseng, Y.T., 2008. Classification of Seafloor Habitats Using Genetic Programming. In: Giacobini, M., Brabazon, A., Cagnoni, S., Di Caro, G.A., Drechsler, R., Ek´art, A., Esparcia-Alc´azar, A.I., Farooq, M., Fink, A., McCormack, J., O'Neill, M., Romero, J., Rothlauf, F., Squillero, G., Uyar, A.S¸., Yang, S. (eds.) EvoWorkshops 2008. LNCS, vol. 4974, pp. 315–324. Springer, Heidelberg.

Skarke, A., Trembanis, A.C., 2011. Parameterization of bedform morphology and defect density with fingerprint analysis techniques. Continental Shelf Research 31, 1688-1700.

Sleath, J.F.A., 1982. The suspension of sand by waves. Journal of Hydraulic Research 20, 439-452.

Sleath, J.F.A., Wallbridge, S., 2002. Pickup from rippled beds in oscillatory flow. Journal of Waterway, Port, Coastal, and Ocean Engineering 128, 228-237.

Smith, J. J., Wiberg, P. L., 2006. Ripple Geometry in Wave-Dominated Environments

Revisited, paper presented at Eos Trans. AGU, 87(36), Ocean Sci. Meet. Suppl., Abstract OS35D-24.
Soulsby, R.L., Whitehouse, R.J.S., 2005. Prediction of ripple properties in shelf seas. Mark 2 Predictor for time evolution. Report TR154, HR Wallingford, Wallingford, UK. http://eprints.hrwallingford.co.uk/281/
Soulsby, R.L., Whitehouse, R.J.S., Marten, K.V., 2012. Prediction of time-evolving sand ripples in shelf seas. Continental Shelf Research 38, 47-62.
Southard, J. B., Lambie, J., Federico, D., Pile, H., Weidman, C., 1990. Experiments on bed configurations in fine sands under bidirectional purely oscillatory flow, and the origin of hummocky cross-stratification. Journal of Sedimentary Petrology, 60(1), 1–17
Styles, R., Glenn, S.M., 2002. Modeling bottom roughness in the presence of wave-generated ripples. Journal of Geophysical Research, 107(C8), doi:10.1029/2001JC000864
Thorne, P.D., Williams, J.J., Davies, A.G., 2002. Suspended sediments under waves measured in a large-scale flume facility. Journal of Geophysical Research, 107(C8), doi:10.1029/2001JC000988
Thorne, P.D., Davies, A.G., Bell, P.S., 2009. Observations and analysis of sediment diffusivity profiles over sandy rippled beds under waves. Journal of Geophysical Research, 114, C02023, doi:10.1029/2008JC004944
Traykovski, P., 2007. Observations of wave orbital scale ripples and a nonequilibrium time-dependent model. Journal of Geophysical Research 112, C06026, doi:10.1029/2006JC003811.
Traykovski, P., Hay, A.E., Irish, J.D., Lynch, J.F., 1999. Geometry, migration, and evolution of wave orbital ripples at LEO-15. Journal of Geophysical Research 104(C1), 1505–1524, doi:10.1029/1998JC900026.
Trembanis, A.C., Wright, L.D., Friedrichs, C.T., Green, M.O., Hume, T., 2004. The effects of spatially complex inner shelf roughness on boundary layer turbulence and current and wave friction: Tairua embayment, New Zealand. Continental Shelf Research 24, 1549-1571.
van Maanen, B., Coco, G., Bryan, K.R., Ruessink, B.G., 2010. The use of artificial neural networks to analyze and predict alongshore sediment transport. Nonlinear Processes in Geophysics: 17, p. 395-404. doi:10.5194/npg-17-395-2010
Van Rijn, L.C., 1993. Principles of sediment transport in rivers, estuaries and coastal seas. Aqua publications Amsterdam.
Werner, B.T., Kocurek, G., 1999. Bedform spacing from defect dynamics. Geology 27, 727-730.
Whigham, P.A., Recknagel, F., 1999. Predictive modelling of plankton dynamics in freshwater lakes using genetic programming. In: MODSIM 1999 International Congress on Modelling and Simulation, Modeling and Simulation Society of Australia and New Zealand, 6–9 December, 1999, New Zealand, pp. 691–696.
Wiberg, P.L., Harris, C.K., 1994. Ripple geometry in wave-dominated environments. Journal of Geophysical Research 99(C1), 775-775, doi:10.1029/93JC02726.
Wikramanayake, P.N., Madsen, O.S., 1991. Calculation of movable bed friction factors. Technical Report. Massachusetts Inst. of Technol., Cambridge, Massachusetts, 105 pp.

Williams, J.J., Bell, P.S., Thorne, P.D., Trouw, K., Hardcastle, P.J., Humphery, J.D., 2000. Observed and predicted vertical suspended sediment concentration profiles and bedforms in oscillatory-only flow. Journal of Coastal Research, 698-708.
Williams, J.J., Bell, P.S., Thorne, P.D., 2005. Unifying large and small wave-generated ripples. Journal of Geophysical Research 110, C02008, doi:10.1029/2004JC002513.
Williams, J.J., Bell, P.S., Thorne, P.D., Metje, N., Coates, L.E., 2004. Measurement and prediction of wave-generated suborbital ripples. Journal of Geophysical Research 109, C02004, doi:10.1029/2003JC001882.
Xu, J.P., 2005. Observations of plan-view sand ripple behavior and spectral wave climate on the inner shelf of San Pedro Bay, California. Continental Shelf Research 25, 373-396.
Yamaguchi, N., Sekiguchi, H., 2011. Variability of wave-induced ripple migration in wave-flume experiments and its implications for sediment transport. Coastal Engineering 58, 671-677.
Yan, B., Zhang, Q.H., Wai, O.W.H., 2008. Prediction of sand ripple geometry under waves using an artificial neural network. Computers & Geosciences 34, 1655-1664.
You, Z.-J., Yin, B., 2006. A unified criterion for initiation of sediment motion and inception of sheet flow under water waves. Sedimentology 53, 1181-1190.

FIGURES AND TABLES

Table 1: Data Summary; Measurement numbers reported are the ripple length measurements used in our study. Measurements with both length and height are less.

Authors	Setting	Measurements	T (s)	U (m/s)	d_0 (m)	D_{50} (m)
Boyd et al. 1988	Field	36	3.8-9.8	0.04-0.28	0.05-0.60	0.00011
Cummings et al. 2009	Wave Racetrack	14	4.4-14	0.37-1.22	0.95-4.50	0.00012-0.0008
Delgado Blanco et al. 2004	Wave Flume	17	6.0	0.14-0.74	0.27-1.42	0.00035
Doucette 2000	Field	49	4.7-12.2	0.15-0.52	0.31-1.93	0.00015-0.00053
Doucette 2002	Field	25	2.2-12.2	0.17-0.66	0.31-2.22	0.00035-0.00062
Doucette and O'Donoghue 2006	Osc. Tunnel	32	2.0-12.2	0.29-0.63	0.24-2.00	0.00044
Dumas et al. 2005	Osc. Tunnel	23	7.9-11.0	0.21-1.26	0.51-4.17	0.00011-0.00023
Grasmeijer and Kleinhans 2004	Field	26	4.0-10.5	0.23-0.84	0.58-2.41	0.00024
Hanes et al. 2001	Field	169	7.1-19.7	0.92-1.11	0.47-5.02	0.00012-0.00166
Hume et al. 1999	Field	9	11.0	0.08-0.37	0.30-1.30	0.00040
Inman 1957	Field	59	0.5-15.0	0.06-0.94	0.04-2.74	0.00008-0.00091
Kennedy and Falcon 1965	Wave Flume	10	1.1-2.0	0.12-0.26	0.04-0.13	0.00010-0.00032
Miller and Komar 1980a	Wave Flume	4	3.0-8.0	0.05-0.34	0.14-0.54	0.00017
Miller and Komar 1980b	Field	26	6.0-18.2	0.03-0.41	0.07-2.14	0.00017-0.00029
Mogridge 1972	Osc. Tunnel/ W. Flume	72	1.0-14.0	0.13-0.68	0.05-1.84	0.00036
O'Donoghue and Clubb 2001	Osc. Tunnel	35	2.0-15.0	0.25-0.94	0.16-2.92	0.00018-0.00044
O'Donoghue et al. 2006	Osc. Tunnel	27	3.1-12.5	0.31-0.85	0.42-2.70	0.00022-0.00044
Pedocchi and García 2009b	Osc. Tunnel	22	2.0-18.0	0.20-1.00	0.16-2.86	0.00025
Ribberink and Al-Salem 1994	Osc. Tunnel	25	2.0-10.0	0.30-1.50	0.31-3.82	0.00021
Sleath 1982	Osc. Tunnel	13	2.9-5.1	0.16-0.44	0.17-0.51	0.00020-0.00041
Sleath and Wallbridge 2002	Osc. Tunnel	26	2.8-5.	0.08-0.77	0.12-0.80	0.00020-0.00080
Southard et al. 1990	Osc. Tunnel	63	93.1-19.3	0.16-1.00	0.26-3.56	0.00011-0.00032
Thorne et al. 2002	Wave Flume	14	4.0-6.0	0.26-0.66	0.41-1.05	0.00033
Williams et al. 2000	Wave Flume	9	4.8-5.3	0.19-0.69	0.30-1.10	0.00016-0.00033
Williams et al. 2004	Wave Flume	65	4.0-6.0	0.13-1.02	0.25-1.96	0.00016-0.00035
Xu 2005	Field	13	8.9-14.8	0.11-0.16	0.41-0.76	0.00009
Yamaguchi and Sekiguchi 2011	Wave Flume	111	1.3-5.0	0.18-0.51	0.07-0.55	0.00032-0.00073

Figure 1: A schematic phase diagram of oscillatory bedforms. O, S, and A represent orbital, suborbital, and anorbital ripples respectively: smaller steep ripples that occur under small/moderate hydrodynamic forcing in fine sands. Orbital, suborbital and Anorbital ripples occur in sequence as hydrodynamic forcing is increased. Recent data collection campaigns have focused on 1) strong hydrodynamic forcing in fine sands ('hummocks' or 'long wave ripples') and 2) steep, large ripples in coarse sand. Modified after Cummings et al., (2009). Question marks denote the unknown threshold for plane bed in coarse grained environments, and unknown potential for coarse grained environments to be sculpted into long wavelength 'hummocky' ripples. Additionally it is unknown if suborbital and anorbital scale ripples exist in coarse grain settings. Lower plane bed conditions are likely only applicable for laboratory studies where the bed is artificially flattened (field conditions retain relict or antecedent bed geometry).

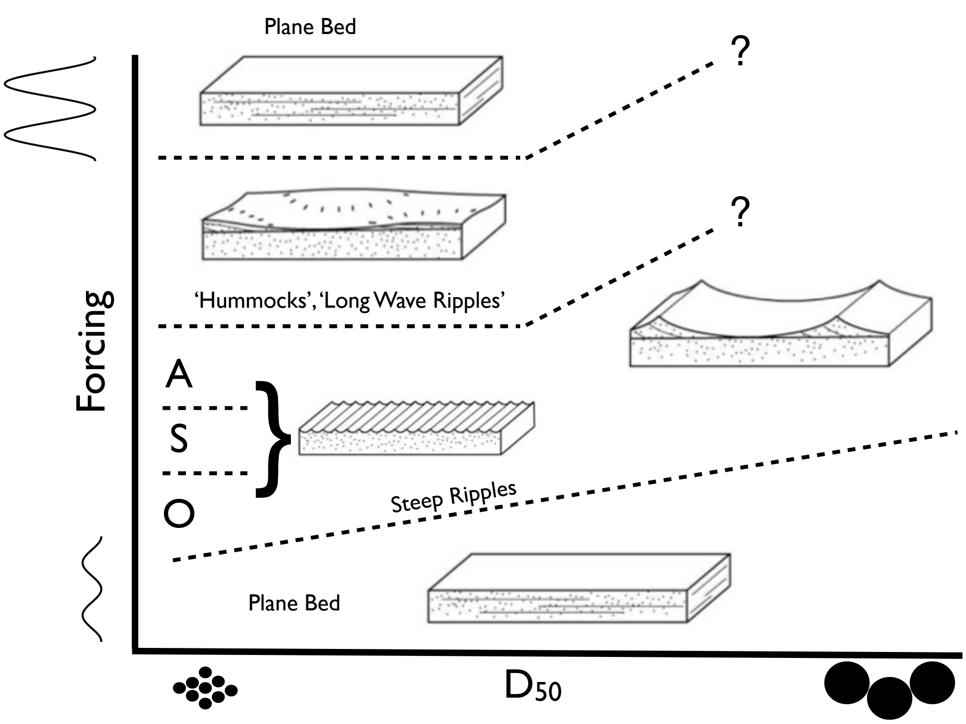

Figure 2: Histograms for ripple length (995 measurements), ripple height (872 measurements), ripple steepness (872 measurements), and for hydrodynamic and sedimentological variables used in this study (includes all 995 data points). Note the different Y-axis values for each graph.

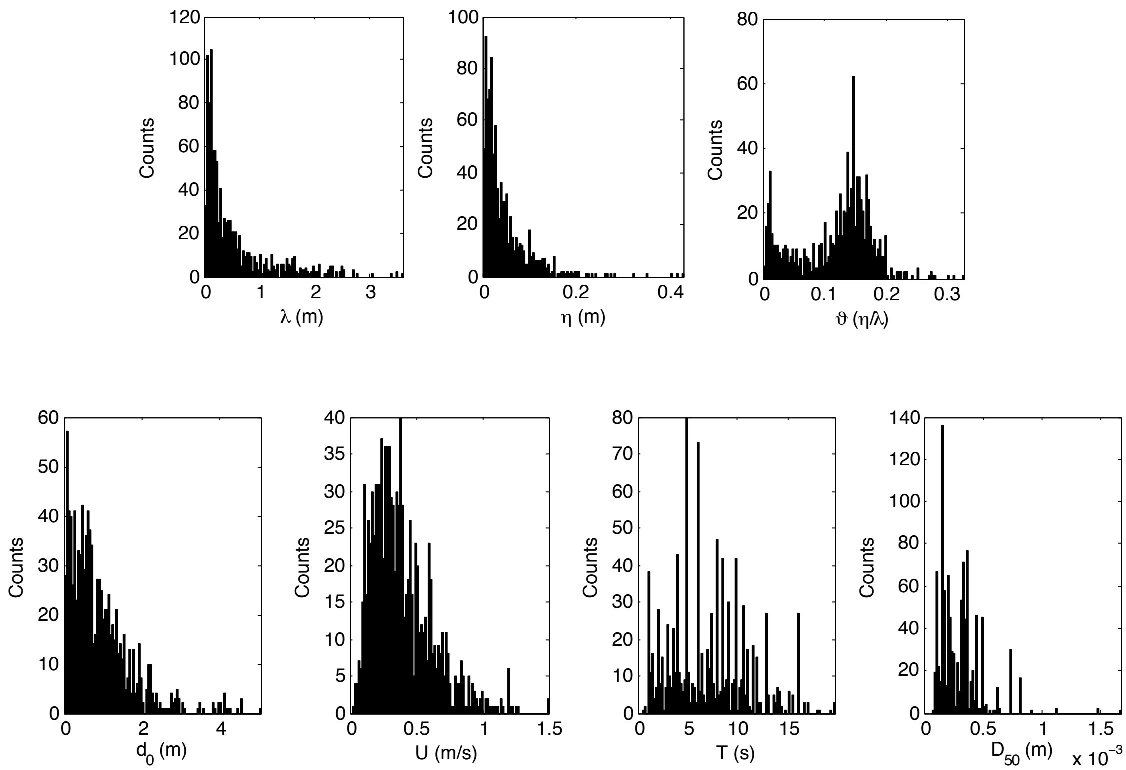

Figure 3: Visualization of the range of forcing conditions in the ripple length dataset. Each plot represents a 2 dimensional projection of the entire data set onto the set of axes shown. For instance, the first panel with data projected onto the U-T plane shows no information about D_{50} or d_0. Ripple height dataset shows qualitatively similar distribution and range, but with fewer data points (872 vs. 995).

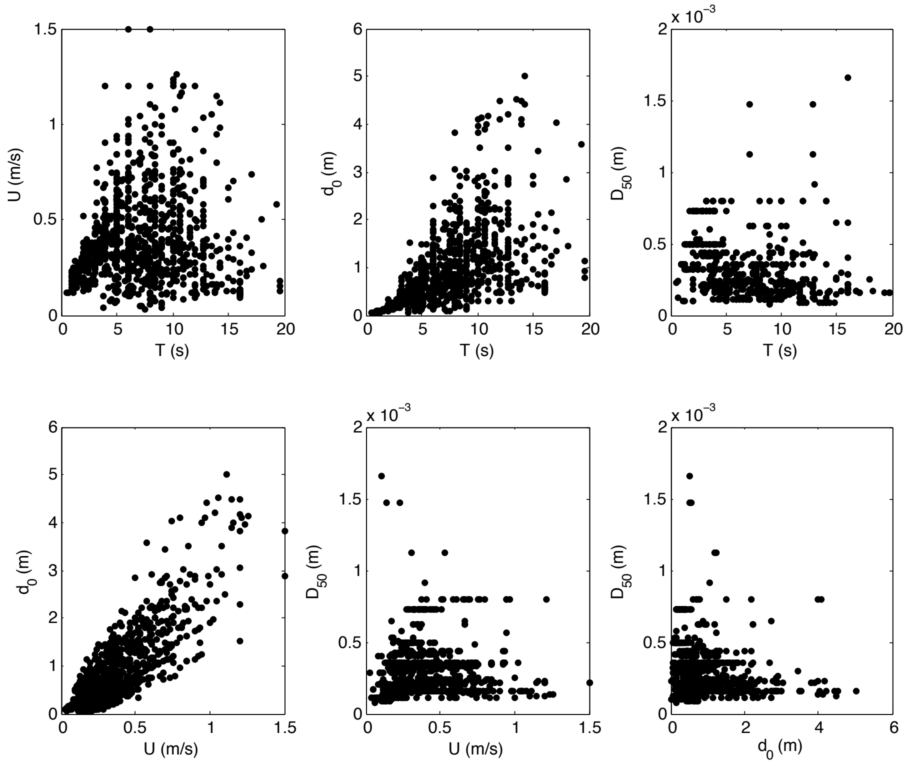

Figure 4: Centroid locations in the ripple length dataset, visualized using the projections shown in Figure 3. Stars denote centroid locations (training data), while points denote unselected data (validation and testing). Note that centroids are distributed throughout the dataset. Centroid locations for the ripple height (and steepness) dataset look qualitatively similar but have more centroids (40 vs. 30) and fewer data points (832 vs. 965).

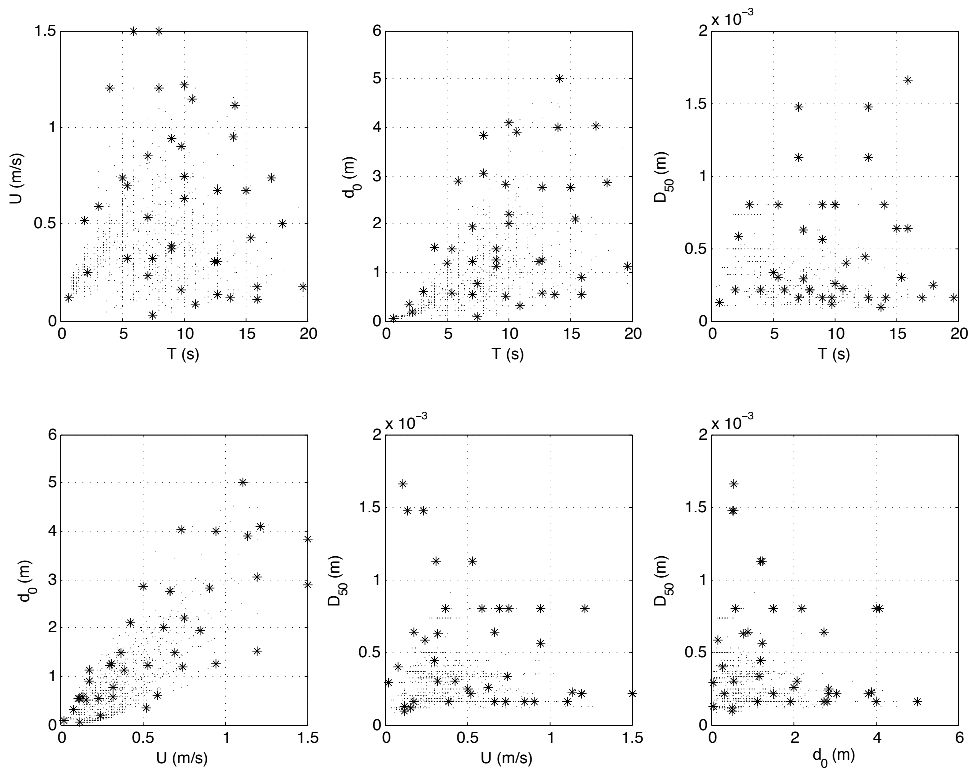

Figure 5: Example of the genetic programming process. Potential solutions are encoded as a population of ‘trees’. Here a hypothetical population of two solutions is shown. The first solution has a low MSE and therefore persists to the next iteration. The second solution has a high MSE and therefore is subject to removal, mutation, or crossover. Here is an example of ‘crossover’ whereby the old solution is combined with parts of other, better performing solutions to create a new potential solution in the next iteration.

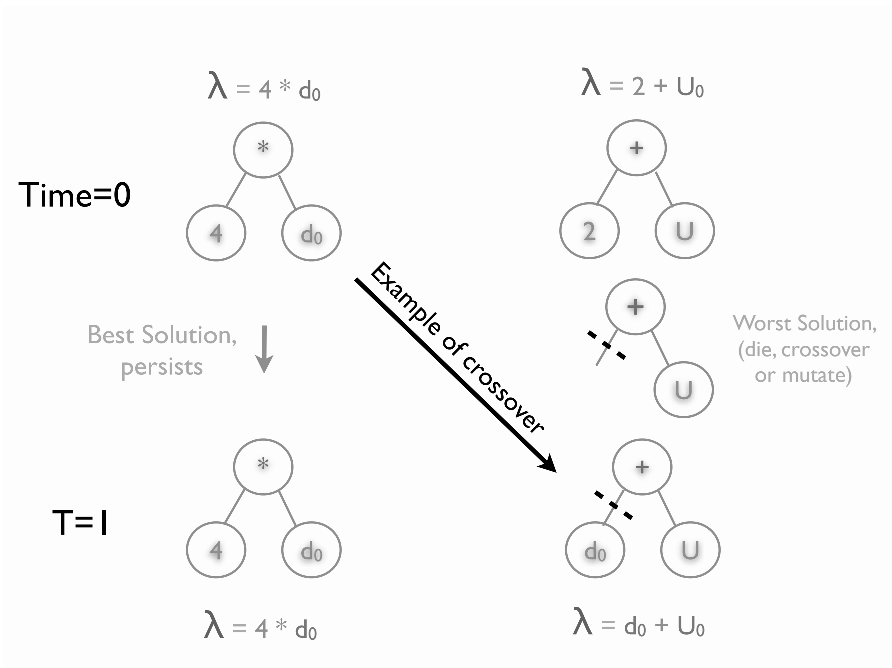

Figure 6: Ripple Length Pareto front; Error is expressed as mean squared error of candidate solution versus the validation data set. Complexity is a quantification of the candidate solution length (both mathematical operators and variables).

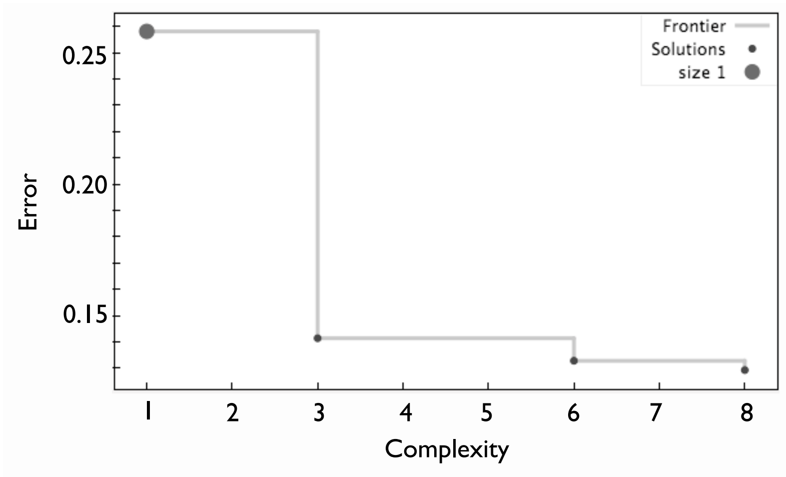

Table 2: Solutions for Ripple Length

Solution	Complexity	MSE
$\lambda = U$	1	0.258
$\lambda = 0.607 d_0$	3	0.141
$\lambda = \dfrac{d_0}{1.39 + (1000 D_{50})}$	6	0.133
$\lambda = \dfrac{d_0}{1.12 + 2.18(1000 D_{50})}$	8	0.129

Figure 7: Example behavior of ripple length predictor as a function of grain size for given bottom orbital excursions (left panel) and as a function of bottom orbital excursion for given grain size (right panel).

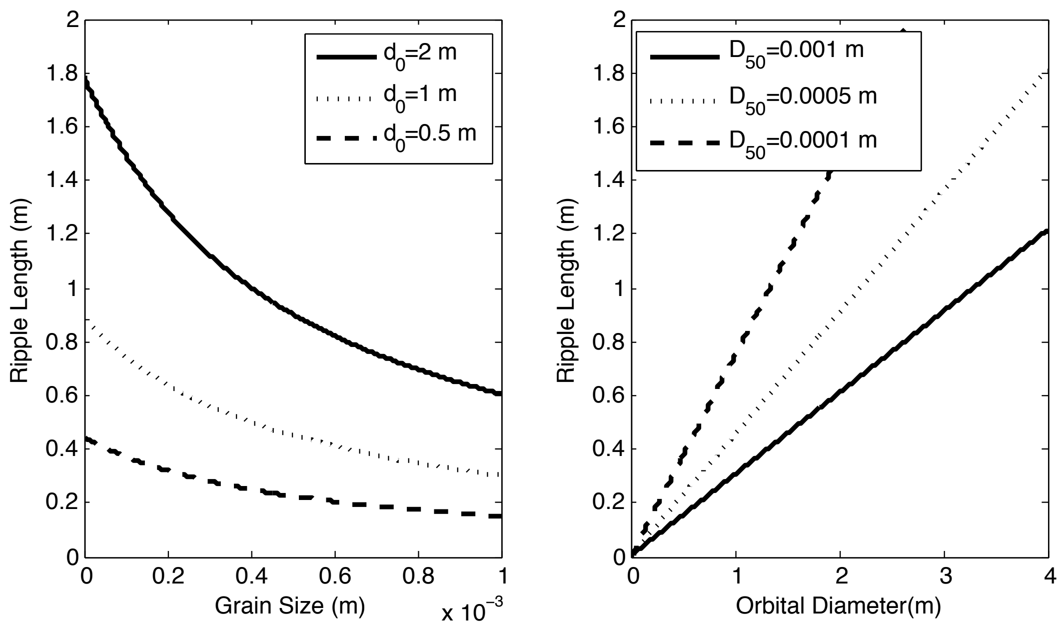

Figure 8: GP predictor of ripple length (8), Soulsby and Whitehouse (2005) predictor (3) and Pedocchi and García (2009a) predictor (5) evaluated using only the independent testing dataset. Top row shows the predictors in linear space, while bottom row shows log-log space.

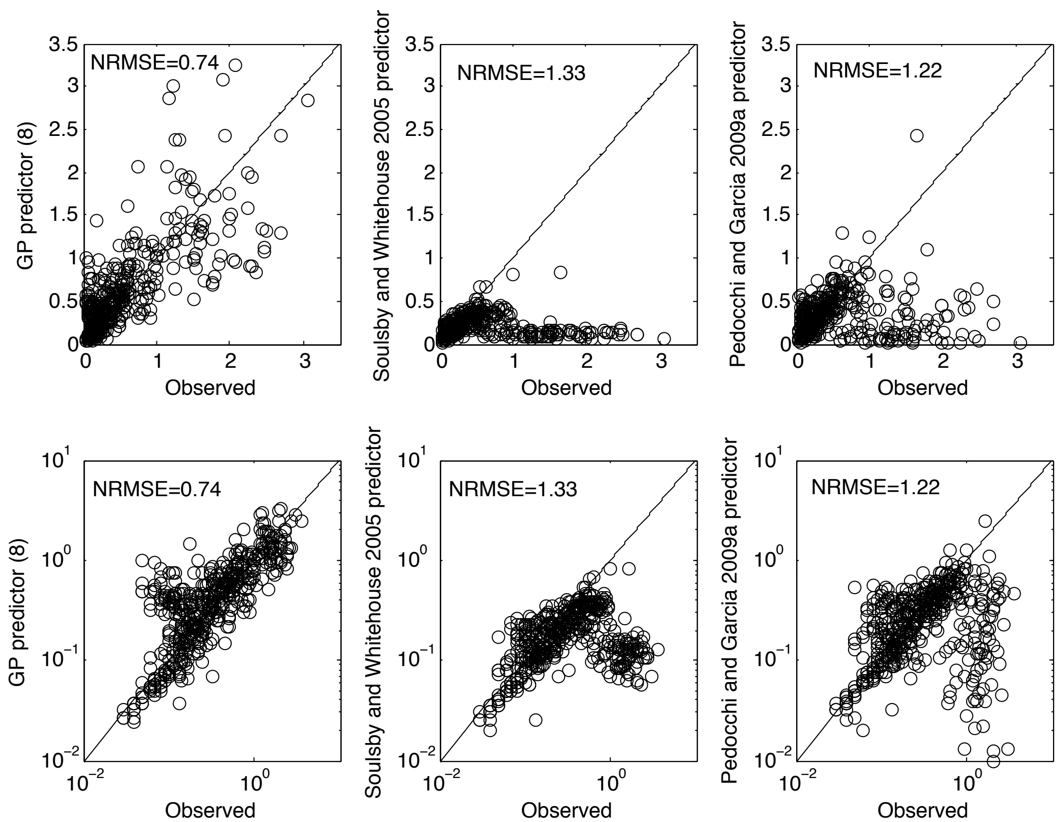

Figure 9: Pareto front for ripple height; Error is mean squared error of candidate solution versus the validation data set. Complexity is a quantification of the candidate solution length (both mathematical operators and variables).

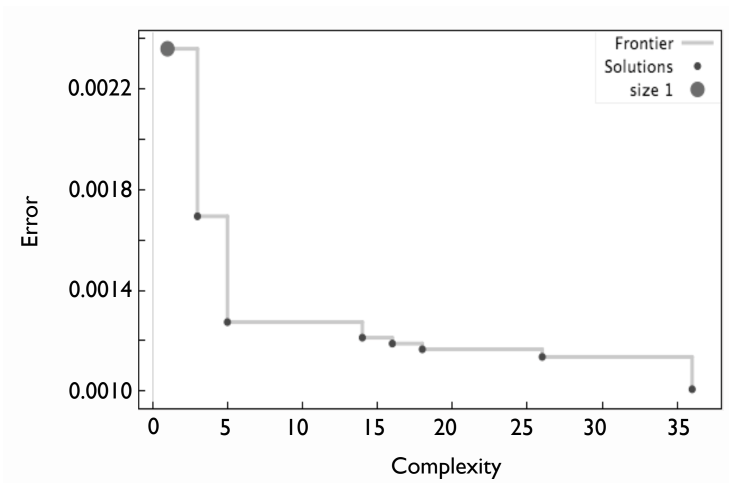

Table 3: Solutions for Ripple Height

Solution	C	MSE
$\eta = 0.435 d_0$	3	0.0017
$\eta = 0.313\lambda(1000D_{50})$	5	0.0013
$\eta = \dfrac{\lambda(1000D_{50})^2}{0.372 + 5.29(1000D_{50})^2}$	14	0.0012
$\eta = \dfrac{\lambda(1000D_{50})^3}{0.0731 + 5.57(1000D_{50})^3}$	18	0.0012
$\eta = \dfrac{0.0237\lambda(1000D_{50}) + \lambda(1000D_{50})^3 - 0.308\lambda(1000D_{50})^2}{0.0332 + 4.46(1000D_{50})^3 - 0.321D_{50}}$	36	0.0010

Figure 10: Example behavior of Ripple height predictor as a function of grain size for given bottom orbital excursions (left panel) and as a function of bottom orbital excursion for given grain size (right panel).

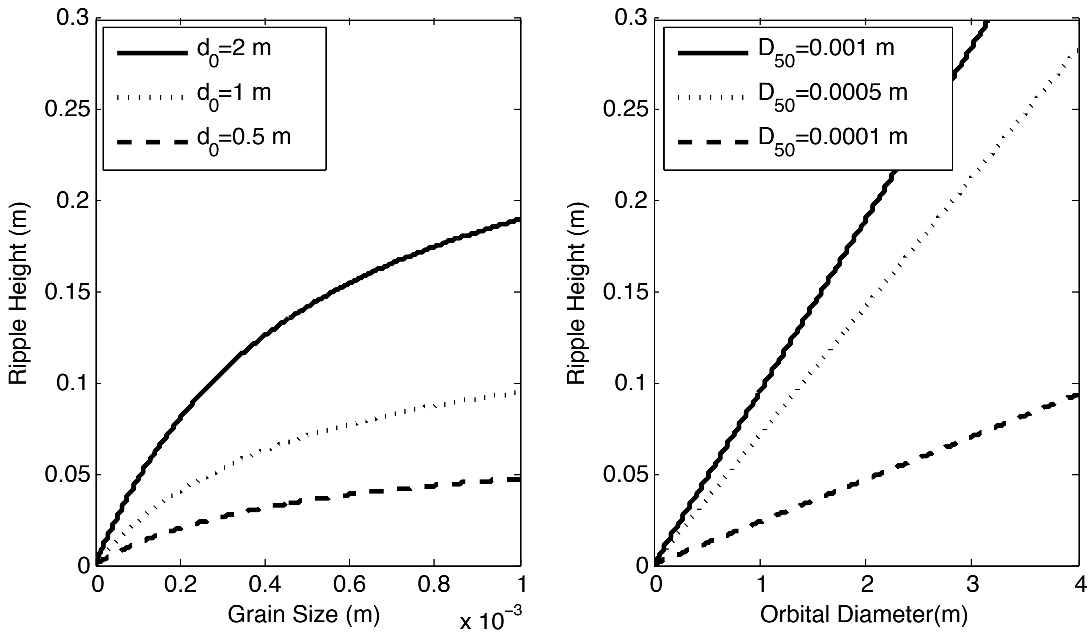

Figure 11: GP predictor of ripple height (10), Soulsby and Whitehouse (2005) predictor (3) and (4) and Pedocchi and García (2009a) predictor (6) evaluated using only the independent testing dataset. Top row shows the predictors in linear space, while bottom row shows log-log space.

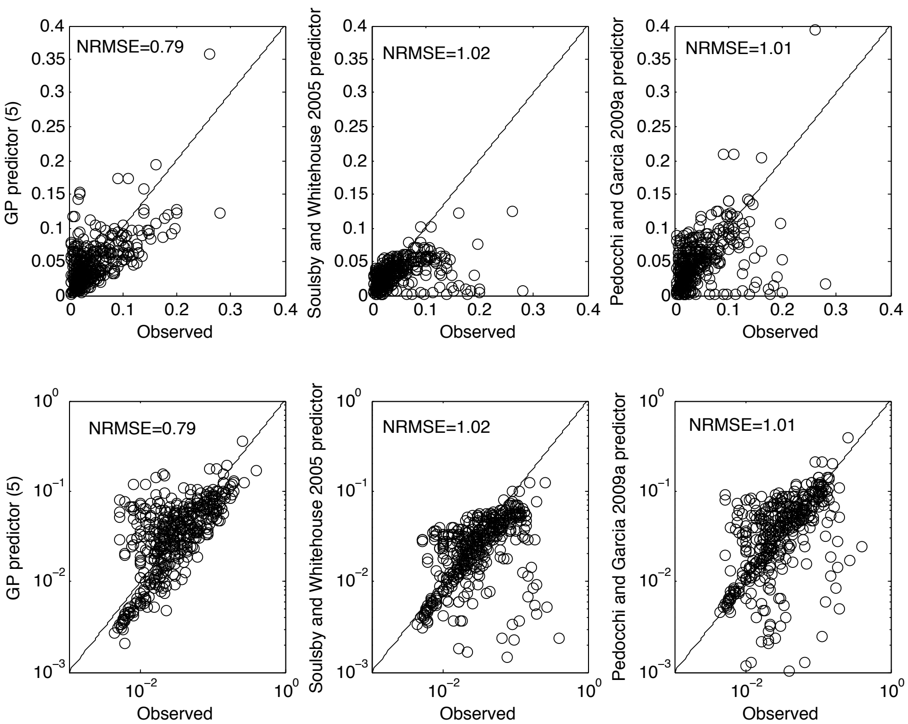

Figure 12: Pareto front for ripple steepness; Error is mean squared error of candidate solution versus the validation data set. Complexity is a quantification of the candidate solution length (both mathematical operators and variables).

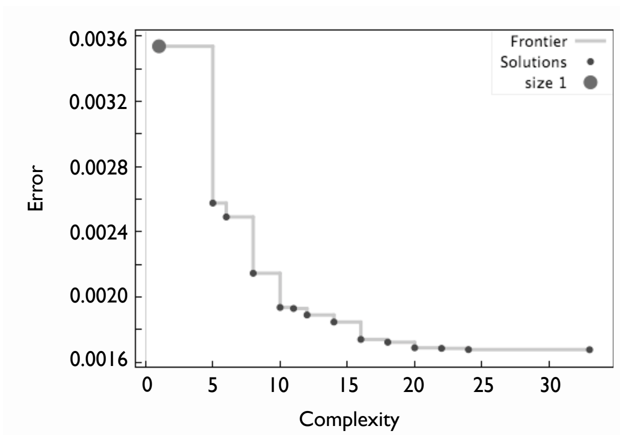

Table 4: Solutions for Ripple Steepness

Solution	C	MSE
$\vartheta = 0.119$	1	0.0035
$\vartheta = 0.154 - 0.0613\lambda$	5	0.0026
$\vartheta = \dfrac{(1000D_{50})}{\lambda + 6.23(1000D_{50})}$	8	0.0021
$\vartheta = \dfrac{3.42}{22 + \left(\dfrac{\lambda}{(1000D_{50})}\right)^2}$	10	0.0019
$\vartheta = \dfrac{0.447}{2.81 + \left(\lambda^2 + \dfrac{-0.617\lambda}{(1000D_{50})}\right)^2}$	16	0.0017

Figure 13: Example behavior of Ripple Steepness predictor as a function of grain size for given bottom orbital excursions (left panel) and as a function of bottom orbital excursion for given grain size (right panel).

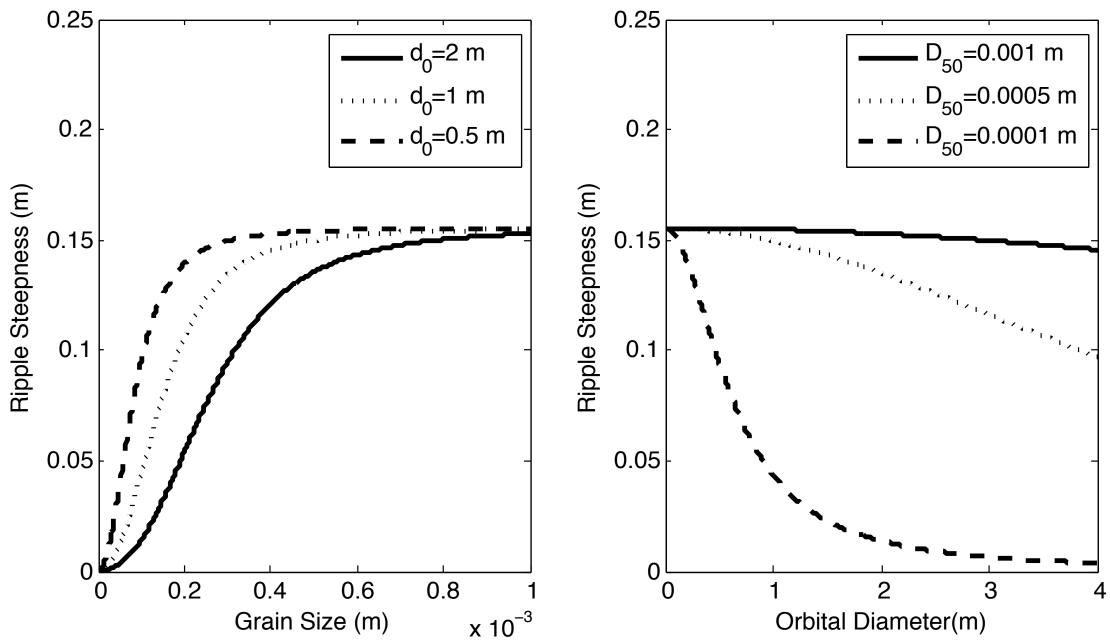

Figure 14: GP predictor of ripple steepness (13), Predictor based on linear convolution of GP height and length (11), Soulsby and Whitehouse (2005) predictor (4) and Pedocchi and García (2009a) predictor (5) and (6) evaluated using only the independent testing dataset. Top row shows the predictors in linear space, while bottom row shows log-log space.